Geometry and electronic structure of monolayer, bilayer, and multilayer Janus WSSe

Wenzhe Zhou,[1,2] Jianyong Chen,[1] Zhixiong Yang,[1] Junwei Liu,[3] and Fangping Ouyang[1,2,*]

[1]*Powder Metallurgy Research Institute, and State Key Laboratory of Powder Metallurgy, Central South University, Changsha 410083, People's Republic of China*

[2]*School of Physics and Electronics, and Hunan Key Laboratory for Super-Microstructure and Ultrafast Process, Central South University, Changsha 410083, People's Republic of China*

[3]*Department of Physics, The Hong Kong University of Science and Technology, Hong Kong, People's Republic of China*

(Received 13 November 2018; revised manuscript received 16 February 2019; published 28 February 2019)

Newly synthesized Janus transition-metal dichalcogenides *MXY* (M = Mo, W; $X \neq Y$ = S, Se, Te) possess intrinsic Rashba spin splitting and out-of-plane dipole moment due to the breaking of mirror symmetry. Taking WSSe as an example, we present a first-principles investigation of the structural stability and electronic properties of mono-, bi-, and multilayer *MXY*. Results show that S atoms contribute more than Se atoms in the valence-band maximum at the Γ point, which can be greatly affected by interlayer interactions. The high-symmetry AA′ stacking is still the most stable pattern, but there are various orders of chalcogen atomic layers in each stacking. The most preferred order of two adjacent layers is S-Se-Se-S, followed by Se-S-Se-S. The Se-S-Se-S–ordered WSSe bilayer is found to have significant layer splitting due to the net dipole moment, which has great potential for solar cells. Layer-dependent Rashba splittings exist in asymmetry-ordered WSSe bilayers, that can be tuned by changing the interlayer distance, originating from the regulation of interlayer electrostatic interaction. However, there is not layer splitting in a symmetrically stacked WSSe bilayer and opposite Rashba splitting appears in the two layers at a sufficiently large interlayer distance. The electronic structures and spin splittings can be easily modulated by controlling the chalcogen atomic-layer order, so that we can obtain the desired properties from mono-, bi-, and multilayer *MXY*.

DOI: 10.1103/PhysRevB.99.075160

I. INTRODUCTION

Transition-metal dichalcogenides, with the formula of MX_2, have attracted much attention both in experimental and theoretical research [1], facilitated by some extraordinary physics, for instance, the degenerate but inequivalent valleys caused by the inverse symmetry breaking [2], the considerable spin splitting at the valence-band maximum owing to the strong spin-orbit coupling (SOC) of the transition-metal atom, and different circular polarizations of optical excitation [3,4]. These important distinctions from other atomically thin layered materials give MX_2 unique advantages in the study of valleytronics [5], spintronics, optoelectronics, etc.

Monolayer semiconducting MX_2 consists of two layers of chalcogen atom and one layer of transition-metal atom with ABA stacking, and thus exhibits mirror reflection symmetry with SOC-caused spin splitting only in the out-of-plane direction [6]. Using a distinctive synthetic method, Li *et al.* replace the top-layer S with Se atoms, obtaining the Janus monolayer of MoSSe [7]. The Janus monolayers of transition-metal dichalcogenides (*MXY*) break the mirror symmetry that brings a vertical dipole and enhanced Rashba spin-orbit coupling [8]. To our satisfaction, *MXY* preserve the excellent features of MX_2, which extend the applications of transition-metal chalcogenides. It has been predicted that *MXY* can be efficient photocatalysts for water splitting [9,10] and piezoelectric two-dimensional (2D) materials in device applications [11] due to the intrinsic out-of-plane dipoles. In addition, some methods have been carried out on the manipulation of the spin splitting and valley polarization in these *MXY* materials, such as electric field [12], strain [13], and magnetic doping [14].

Far from what we expected, the Zeeman splitting in bilayer $MoTe_2$ indicates that the layer is also an important degree of freedom in those 2D materials [15]. Other studies also showed that we can regulate the electronic structures of MX_2 by layer control [16]. The orbital projected band structures of MX_2 monolayers show that the p_z orbits of chalcogen atoms contribute a large proportion to the states of the valence-band maximum (VBM) at Γ and the conduction-band minimum (CBM) of a point between Γ and K [17]. The interlayer interaction has a particularly important effect on the p_z orbits of chalcogen atoms, leading to the great band splitting at those two points, which is the reason for the direct-indirect transition from monolayer to few layers [18]. The interlayer van der Waals (vdW) interaction is related to two factors: distance and atomic species. The former can be tuned by changing the stacking patterns of few-layer MX_2, which is an efficient way to regulate and control the electronic and optical properties [19].

As for *MXY*, different chalcogen atoms are destined to play different roles in a *MXY* monolayer, thus brings multilayers more stacking styles with multifarious electronic structures. Taking WSSe as an example of polar transition-metal dichalcogenides, this work is mainly aimed to illustrate the electronic structures of the WSSe monolayer, bilayers, and

*ouyangfp06@tsinghua.org.cn

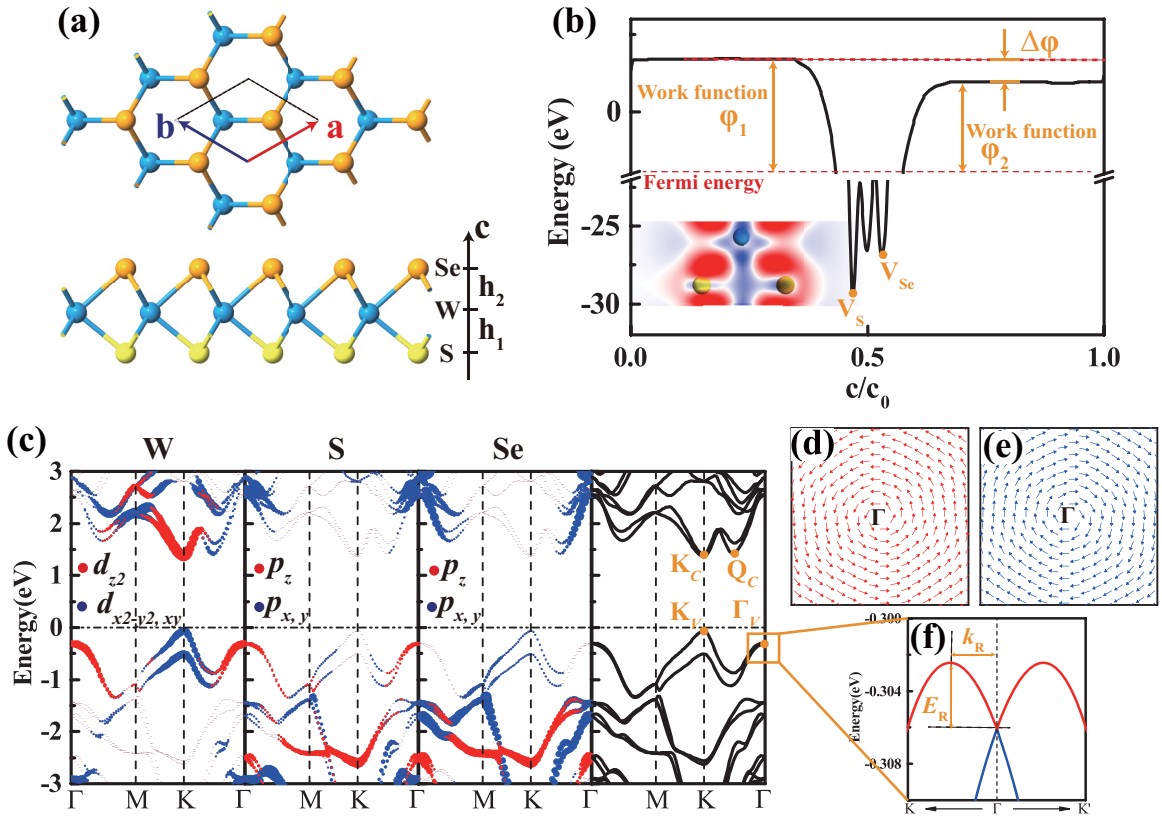

FIG. 1. (a) The optimized structure of the WSSe monolayer. (b) The average electronic potential energy in the vertical direction of the WSSe monolayer. The inset is the differential charge density, where the red and blue mean accumulation and depletion of electrons, respectively. (c) The projected band structures of the WSSe monolayer with SOC. (d),(e) The in-plane spin-polarization components of two bands around $\mathbf{\Gamma}_V$. (f) Magnified view of the band structure around $\mathbf{\Gamma}_V$.

multilayers through first-principles calculations. The most favorable stacking order is determined and the interlayer interaction and spin-orbit coupling induced layer and spin splittings are also explored.

II. COMPUTATIONAL DETAILS

In this paper, the structural optimization and the iterative calculations are all performed through the Vienna *ab initio* Simulation Package (VASP) based on density functional theory (DFT) [20], which is particularly adapted to research the electronic structures of various materials [21–23]. The projector augmented wave (PAW) scheme and plane-wave basis with an energy cutoff of 500 eV are used [24]. The exchange-correlation energy is treated by generalized gradient approximation using the Perdew-Burke-Ernzerhof functional [25]. Dipole correction is applied to correct the errors introduced by the periodic boundary conditions [26]. We consider the DFT-D2 approach to deal with vdW interactions [27], which yield very good interlayer distances [19] and can well describe long-range vdW interactions in these *MXY* systems [10]. The spin-orbit interaction is contained to discuss the phenomena of spin splitting. All the optimization and self-consistent iteration are finished until the force on each atom and the energy difference between two electronic steps are less than 0.005 eV/Å and 10^{-8} eV, respectively. $15 \times 15 \times 1$ Γ-centered k mesh and vacuum region of 30 Å along the c direction are set to ensure that the results are sufficiently accurate.

III. RESULTS AND DISCUSSION

A. WSSe monolayer

The WSSe monolayer is constructed by a WS_2 monolayer with one layer of S atoms replaced by Se atoms. It still exhibits a hexagonal lattice, from the top view in Fig. 1(a). However, the point groups of MX_2 and MXY monolayers are D_{3d} and C_{3v}, respectively. The high-symmetry points in reciprocal space are Γ (0, 0, 0), M (0.5, 0, 0), and K (1/3, 1/3, 0). The optimized lattice constant of monolayer WSSe is $a = b = 3.247$ Å. The covalent bonds of W-S and W-Se are different, and the distance between the three atomic layers is $h_1 = 1.53$ Å, $h_2 = 1.71$ Å. The bond lengths in monolayer WSSe are all between those in WS_2 and WSe_2. The average electric potential energy and the differential charge density in the c direction are shown in Fig. 1(b).

Compared with MX_2, the breaking of the mirror symmetry in the vertical direction results in the different work function of about 0.738 eV on two sides ($\Delta\varphi$). The S and Se atoms get electrons from the W atoms, but the potential energy is smaller and the work function is larger on the S side than those on the

TABLE I. The orbital compositions at energy valleys (K_C, K_V, Γ_V, Q_C) of the WSSe monolayer.

	K_C	K_C	Γ_V	Q_C
W-d_{z^2}	83.5%	0	74.6%	10.3%
W-$d_{x^2-y^2}$, W-d_{xy}	0	80.3%	0	52.1%
S-p_z	0	0	15.4%	2.14%
S-p_x, S-p_y	2.32%	7.28%	1.06%	7.71%
Se-p_z	0	0	2.52%	2.43%
Se-p_x, Se-p_y	2.56%	10.3%	1.33%	12.7%

Se side ($V_S < V_{Se}$, $\varphi_1 > \varphi_2$). The inset in Fig. 1(b) shows the differential charge density of the WSSe monolayer, indicating that S and Se atoms get electrons from W atoms. This result is different from the WSeTe monolayer [12]. Se atoms get more electrons than the Te atoms in the WSeTe monolayer, but the potential energy and work function are larger on the Se side. This difference may come from the larger electronegativity of the S atom. The electron accumulation increases the potential energy and work function on that side, leading to the larger work function on the S side in the WSSe monolayer and the Se side in the WSeTe monolayer. However, the potential energy on the side of the S atom is too small, corresponding to larger electronegativity, which cannot be offset by the electron accumulation. So the potential energy is smaller at S atoms in a WSSe monolayer but larger at Se atoms in a WSeTe monolayer.

The calculated band structures of monolayer WSSe are shown in Fig. 1(c). Similar to MX_2, the WSSe monolayer is a semiconductor with a direct band gap of 1.423 eV, which is smaller than that of WS_2 (1.552 eV) and larger than that of WSe_2 (1.257 eV). The conduction-band minimum (CBM) and valence-band maximum (VBM) are all at the K point. There are also some special energy valleys, marked as K_C, K_V, Q_C, Γ_V, and large spin splitting at K_V. The atomic orbital projected band structures are calculated. As we expected, different valleys are composed of various atomic orbitals, and there is much difference between the S atom and Se atom. The orbital compositions at valleys are listed in Table I. Like MX_2, K_V and Q_C are composed of in-plane orbitals and K_C and Γ_V consist of out-of-plane orbitals. But by comparing different chalcogen atoms, it is found that Se atomic orbitals mainly contribute to K_V and Q_C, while S atomic orbitals have a greater contribution to Γ_V. This result determines how the interlayer interactions affect the electronic structures of WSSe multilayers.

A significant property of the WSSe monolayer distinguished from mirror symmetric transition-metal dichalcogenides is the existence of Rashba spin splitting. The Rashba SOC effects mainly have two important features: the splitting of the energy band and in-plane spin. The split band structure and spin texture around Γ_V due to Rashba effects are shown in Figs. 1(d)–1(f). The spins of the two topmost valence bands are opposite and satisfy $\sigma(-k) = -\sigma(k)$. The Rashba parameter can be approximated to the formula $\alpha_R = 2E_R/k_R$, where E_R and k_R are the splitting of the energy and wave vector marked in Fig. 1(f). The Rashba parameter and the splitting energy of the WSSe monolayer are 166 meV Å and 3.64 meV.

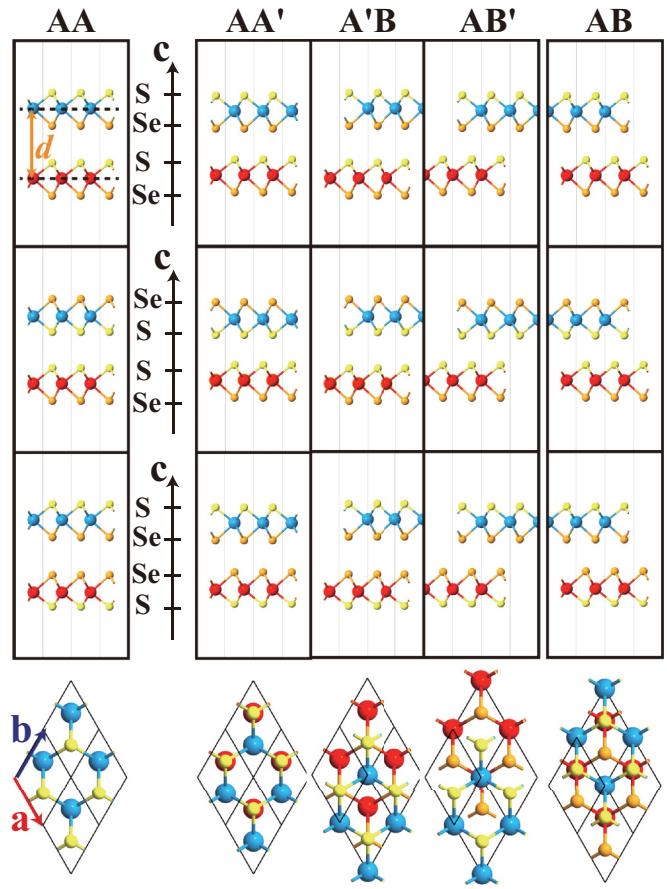

FIG. 2. Diagrams of the atomic structures of high-symmetry WSSe bilayers and each stacking style with three different orders of chalcogen layers. The upper three rows and the bottom row are side and top views, respectively. The big blue and red balls all represent W atoms, and the small yellow and orange balls represent S atoms and Se atoms, respectively.

B. WSSe bilayers

In this study, five high-symmetry stacking orders denoted by AA, AA′, A′B, AB′, and AB are considered, as the same nomenclature in Ref. [28]. Because of the difference between S and Se, there are three different orders of chalcogen layers with each stacking, depicted in Fig. 2. Since every single layer is formed by covalent interactions which are much stronger than the vdW interactions, the in-plane lattice constants are kept fixed in calculations with dipole and vdW corrections. The interlayer distance, ground-state energy, and binding energy of the bilayers from two isolated monolayers are listed in Table II. The interlayer distance is significantly reduced under the vdW correction, indicating the great influence of the vdW attraction. With the same order of chalcogen layers, AA′ and AB are the most preferred stacking patterns with smaller interlayer distance and ground-state energy. Without vdW interaction, the existence of the dipole moment makes the electrostatic potential energy of Se-S-Se-S structures smaller. However, with the effect of vdW interactions, the most stable order of chalcogen layers changes from Se-S-Se-S to S-Se-Se-S, which is the result of the competitions between the vdW interactions and the electrostatic interactions. The vdW

TABLE II. The interlayer distance d_0 (Å), relative ground-state total energy ΔE_0 (meV, with respect to the Se-S-Se-S structure of AA′ stacking) of WSSe bilayers and binding energy E_b (meV). The values in parentheses are the results under dipole and DFT-D2 corrections, while the values outside parentheses are obtained without corrections.

	Without corrections (With corrections)								
	Se-S-Se-S			Se-S-S-Se			S-Se-Se-S		
	d_0	ΔE_0	E_b	d_0 (Å)	ΔE_0	E_b	d_0	ΔE_0	E_b
AA	7.89 (6.86)	1.42 (110.6)	4.62 (192.2)	7.64 (6.61)	3.63 (123.7)	2.41 (179.1)	8.24 (7.12)	3.66 (98.3)	2.38 (204.5)
AA′	7.53 (6.25)	0.0 (0.0)	6.04 (302.9)	7.21 (5.99)	2.63 (23.6)	3.41 (279.3)	7.81 (6.52)	2.27 (–19.9)	3.77 (322.7)
A′B	7.92 (6.84)	1.19 (106.4)	4.85 (196.5)	7.56 (6.59)	3.52 (119.8)	2.52 (183.0)	8.21 (7.09)	3.48 (93.7)	2.56 (209.2)
AB′	7.54 (6.30)	0.9 (24.8)	5.14 (278.0)	7.24 (5.98)	3.17 (34.9)	2.87 (268.0)	7.82 (6.62)	3.29 (16.4)	2.75 (286.5)
AB	7.54 (6.25)	0.36 (7.5)	5.67 (295.3)	7.24 (5.95)	2.76 (20.0)	3.27 (282.8)	7.82 (6.53)	2.75 (–9.7)	3.29 (312.6)

interaction is attractive, while the electrostatic interaction is repulsive at equilibrium interlayer distance. The covalent radius of the Se atom is much larger than the S atom, which results in a larger instantaneous dipole moment. So the attraction between Se atoms is stronger than that between S atoms. For the Se-S-S-Se structure, the large distance of Se atoms makes the vdW attractive energy larger and the small interlayer distance makes the repulsive electrostatic potential larger. Finally, the ground-state total energy satisfies Se-S-S-Se > Se-S-Se-S > S-Se-Se-S.

After getting the optimized structures, we calculate the electronic structures of the more stable WSSe bilayers (AA′ and AB stacking). The band diagrams are shown in Fig. 3. These electronic structures clearly illustrate the band splitting caused by symmetry breaking. On the one hand, there is obvious layer splitting in WSSe bilayers with the Se-S-Se-S order caused by the dipole moment of the WSSe layer and the asymmetry of the order. The potential energy on the side of the S atomic layer is larger, so the energy of layer II is larger than layer I. Thus, layer I (layer II) contributes the CBM (VBM), which means electrons (holes) prefer to stay in layer I (layer II). So the Se-S-Se-S–ordered WSSe bilayers are similar to type-II heterojunctions and are expected to have a greater efficiency of photoelectric conversion used in solar cells. On the other hand, AA′-stacked bilayers have center inversion symmetry but AB stacked does not, so the band structures of AB-stacked WSSe with symmetric orders still have slight layer splitting, which is the same as binary transition-metal chalcogenides (MX_2).

Previous studies on the properties of MX_2 multilayers show that interlayer interactions mainly affect the p_z orbits of chalcogen atoms, resulting in the splitting of the VBM at the Γ point [6,17]. It also happens in the systems of *MXY* multilayers. The distinction is that *MXY* has two different chalcogen atoms, which determines how interlayer interactions work with different kinds of chalcogen atom-layer sequence. In Se-S-Se-S order, the splitting occurs in interlayer but not intralayer, indicating that the interaction of dipole moments overcomes the effect of electrostatic interaction on the states of Γ_V. However, in Se-S-S-Se and S-Se-Se-S systems, there is great splitting at Q_C and Γ_V caused by interlayer interactions. The electrostatic interaction affects S atoms more than Se atoms in Se-S-S-Se systems, while it affects Se atoms more than S atoms in S-Se-Se-S systems. The contributions of chalcogen atoms differ at Q_C and Γ_V, and thus Se-S-S-Se–ordered WSSe bilayers are indirect semiconductors with CBM at K_C and VBM at Γ_V, while the CBM of the S-Se-Se-S–ordered bilayer WSSe is at Q_C.

As a special property of *MXY*, we concentrate on the Rashba splitting of WSSe bilayers. From the magnified band structures in Fig. 3, the effect of symmetry on spin splitting is further confirmed. With Se-S-S-Se and S-Se-Se-S order, the Rashba spin splittings vanish in AA′-stacked WSSe, which are tiny in AB stacking. On the contrary, layer-dependent Rashba splittings are obvious in Se-S-Se-S–ordered WSSe bilayers, which originates from interlayer electrostatic interaction. The effect of interlayer electrostatic interaction can be regarded as an equivalent electric field. The equivalent electric field is pointing out of each layer. Layer I is subjected to an equivalent electric field from the side of the S atomic layer to the side of the Se atomic layer and the field felt by layer II is from the Se side to the S side, as shown by the red and green arrows in Fig. 4(b). This equivalent electric field from the electrostatic interaction makes the electron accumulate to the S atomic layer in layer I, which increases the gradient of crystal potential and enhances the asymmetry of layer I. As a result of the interlayer electrostatic interaction, the Rashba splitting of layer I increases and that of layer II decreases. At the stable interlayer distance (d_0), the Rashba splitting energy of layer I and layer II are 11.4 meV and close to 0, respectively.

The electrostatic interaction can be tuned by interlayer distance, which further regulates the layer-dependent splittings. With the increase of interlayer distance, the splitting of layer I decreases while that of layer II increases, and gradually reaches the value of the monolayer. On the other hand, the S-Se-Se-S–ordered WSSe bilayer has no layer splitting, while the electronic band structure gradually becomes similar to that

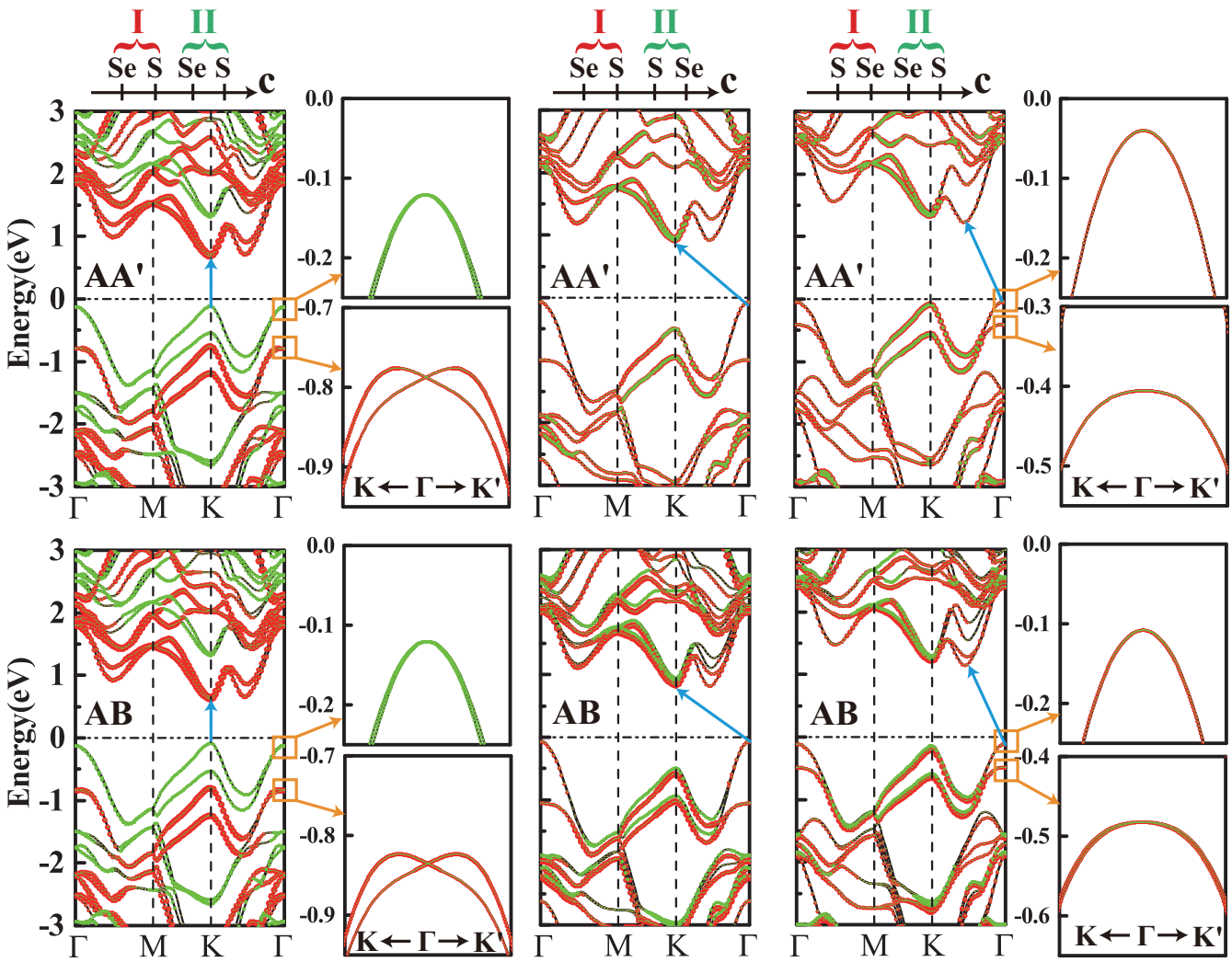

FIG. 3. Band structures of AA′- and AB-stacked WSSe bilayers. Red lines and green lines show the contribution of layer I and layer II, respectively. The magnified views of the band structures of the four valence bands near the Fermi level at the Γ point are illustrated in the small pictures next to the band structures.

of the monolayer with the increase of the interlayer distance. The electronic energies of the states are degenerate, but the spins are in the opposite directions in the two different layers. In S-Se-Se-S–ordered bilayer, it is interlayer interaction that brings about the band splitting at Γ_V and eliminates Rashba splitting, which changes a lot with different interlayer distance. However, the band splitting at Γ_V is caused by the net dipole moment in the Se-S-Se-S–ordered bilayer, which is still quite large at a long distance.

C. WSSe multilayers

It has been established that the stacking pattern plays a decisive role in the electronic structure of WSSe bilayers, and the difference of ground-state energy is just tens of meV. There are many more stacking patterns in WSSe multilayers than in MX_2, and hence we can easily control the structure of multilayer WSSe. Here, we calculate the binding energy of n-layer AA′-stacked WSSe from the *n-1* layer and monolayer, with the formula $E_b = E_{n-1} + E_1 - E_n$, where E_i is the ground-state energy of the i-layer WSSe. Figure 5(a) shows that the binding energy of even-layer WSSe with S-Se-Se-S- … order is smaller than that with Se-S-Se-S- … order, which is contrary in the odd-layer WSSe. The interlayer interaction energy of the Se-Se layers is the smallest, while that of the S-S layer is the largest. S-S layer interaction must be added in the odd-layer WSSe, which is the reason for the larger binding energy with S-Se-Se-S- … order. Meanwhile, with the increase of layers, the proportion of S-S layer interaction also increases. The WSSe multilayers with asymmetric Se-S-Se-S- … order are more stable than that with symmetric S-Se-Se-S- … order, as the difference of ground-state energy between Se-S-Se-S- … order and S-Se-Se-S- … order decreases with the increase of layers. It can be predicted that the most stable n-layer WSSe contain $n-2$ Se-S layer interactions and one Se-Se layer interaction.

The energy band structures of WSSe multilayers with symmetric and asymmetric orders are presented in Fig. 5(b). The total dipole moment is larger, but the layer splitting between adjacent layers in Se-S-Se-S- … systems is smaller

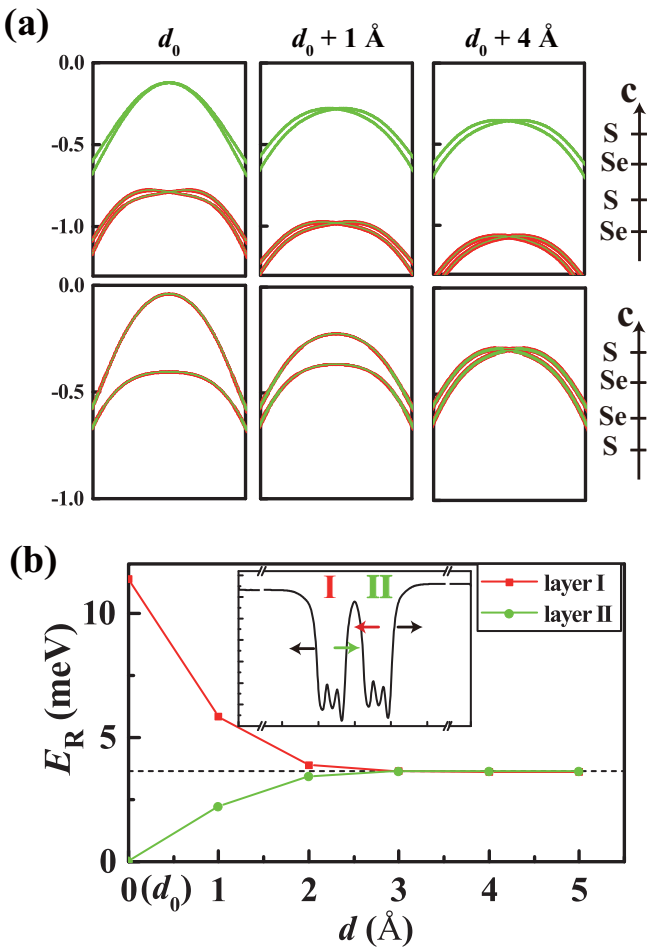

FIG. 4. (a) Four top valence bands near Γ of bilayer WSSe with different interlayer distance. (b) The relationship between the Rashba splitting energy of layer I and layer II in Se-S-Se-S–ordered WSSe bilayer and interlayer distance. The black dashed line indicates the splitting energy of the WSSe monolayer. The insets are the average potential energy with the interlayer distance of $d_0 + 1$ Å. The arrows represent the direction of the local equivalent electric field, where the red and blue indicate the equivalent electric field felt by layer I and layer II, respectively.

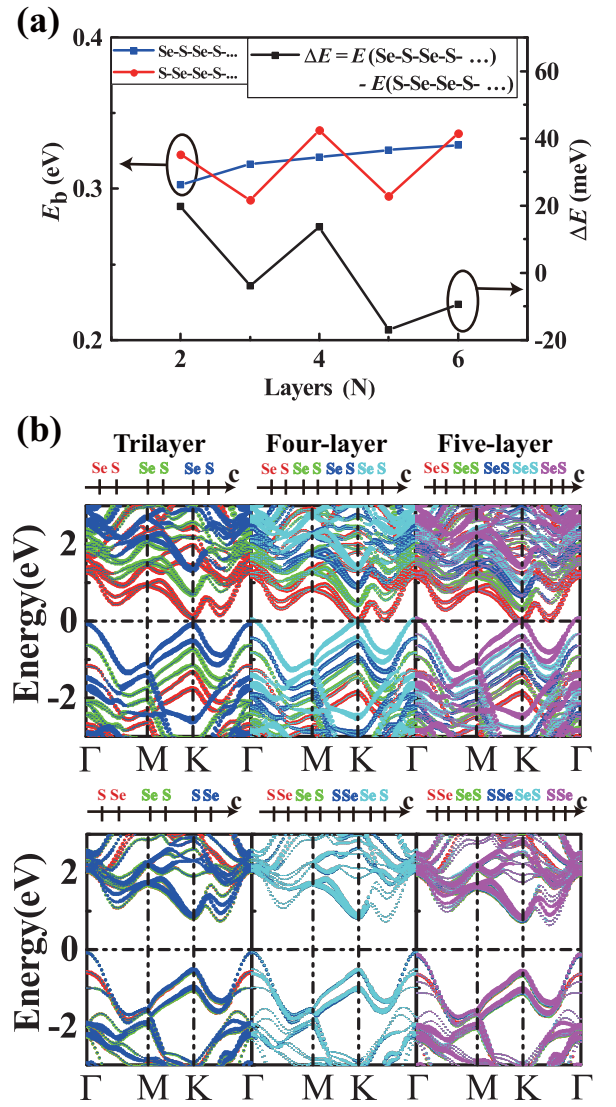

FIG. 5. (a) The binding energy of WSSe multilayers with asymmetric Se-S-Se-S- … order and symmetric S-Se-Se-S- … order (left y axis), and the difference of ground-state energy between Se-S-Se-S- … order and S-Se-Se-S- … order (right y axis). (b) The layer projected band structures of WSSe multilayers.

with the increasing of layers. The charge transfer generated by the dipole moment decreases the dipole effect in turn. When the number of layers is greater than three, the Se-S-Se-S- … ordered multilayers become metals, where there is interlayer charge transfer. In S-Se-Se-S- … ordered multilayers, the layer splitting also exists, but the existence of local symmetry makes the splitting much smaller. It is also observed that S-S interlayer vdW interaction brings greater band splitting at Γ_V and Se-Se interaction increases the splitting at Q_C.

IV. CONCLUSIONS

In summary, the geometries and electronic structures of mono-, bi-, and multilayer WSSe are systematically researched. WSSe is an example of the polar transition-metal dichalcogenides *MXY*. S and Se atoms mainly contribute to Γ_V and Q_C, respectively, which plays a crucial role in band splitting caused by interlayer interactions. S-Se-Se-S is the most preferred order of two adjacent layers. It is found that the band structure of the Se-S-Se-S–ordered WSSe bilayer is similar to that of type-II heterojunctions, which makes it promising for photoelectric conversion devices. In Se-S-Se-S- … ordered systems, the Rashba spin splittings differ in different layers. There is about 11.4 meV Rashba splitting energy in one layer, while almost none in the other layer of the Se-S-Se-S–ordered WSSe bilayer. The layer splitting and layer-dependent Rashba spin splitting can be effectively tuned by interlayer distance. We also explore the stability of WSSe multilayers with multifarious chalcogen atomic-layer order and the most stable order of multilayers is predicted. There is not much difference between the ground-state energies, which means the geometry can be easily tuned. The electronic structures vary with different stacking patterns, and thus we can get the desired properties.

ACKNOWLEDGMENTS

This work is supported by the National Natural Science Foundation of China (Grant No. 51272291), the Distinguished Young Scholar Foundation of Hunan Province (Grant No. 2015JJ1020), the Central South University Research Fund for Innovation-driven program (Grant No. 2015CXS1035), the Central South University Research Fund for Sheng-hua scholars (Grant No. 502033019). J. L. acknowledges financial support from the Hong Kong Research Grants Council (Project No. ECS26302118).

[1] S. Manzeli, D. Ovchinnikov, D. Pasquier, O. V. Yazyev, and A. Kis, Nat. Rev. Mater. **2**, 17033 (2017).

[2] D. Xiao, G.-B. Liu, W. Feng, X. Xu, and W. Yao, Phys. Rev. Lett. **108**, 196802 (2012).

[3] T. Cao, G. Wang, W. Han, H. Ye, C. Zhu, J. Shi, Q. Niu, P. Tan, E. Wang, and B. Liu, Nat. Commun. **3**, 887 (2012).

[4] W. Yao, D. Xiao, and Q. Niu, Phys. Rev. B **77**, 235406 (2008).

[5] J. R. Schaibley, H. Yu, G. Clark, P. Rivera, J. S. Ross, K. L. Seyler, W. Yao, and X. Xu, Nat. Rev. Mater. **1**, 16055 (2016).

[6] A. V. Kolobov and J. Tominaga, *Two-Dimensional Transition-Metal Dichalcogenides* (Springer International Publishing, Switzerland, 2016), p. 168.

[7] A.-Y. Lu, H. Zhu, J. Xiao, C.-P. Chuu, Y. Han, M.-H. Chiu, C.-C. Cheng, C.-W. Yang, K.-H. Wei, and Y. Yang, Nat. Nanotech. **12**, 744 (2017).

[8] Y. Cheng, Z. Zhu, M. Tahir, and U. Schwingenschlögl, Europhys. Lett. **102**, 57001 (2013).

[9] Y. Ji, M. Yang, H. Lin, T. Hou, L. Wang, Y. Li, and S.-T. Lee, J. Phys. Chem. C **122**, 3123 (2018).

[10] Z. Guan, S. Ni, and S. Hu, J. Phys. Chem. C **122**, 6209 (2018).

[11] L. Dong, J. Lou, and V. B. Shenoy, Acs Nano **11**, 8242 (2017).

[12] Q.-F. Yao, J. Cai, W.-Y. Tong, S.-J. Gong, J.-Q. Wang, X. Wan, C.-G. Duan, and J. H. Chu, Phys. Rev. B **95**, 165401 (2017).

[13] T. Hu, F. Jia, G. Zhao, J. Wu, A. Stroppa, and W. Ren, Phys. Rev. B **97**, 235404 (2018).

[14] R. Peng, Y. Ma, S. Zhang, B. Huang, and Y. Dai, J. Phys. Chem. Lett. **9**, 3612 (2018).

[15] C. Jiang, F. Liu, J. Cuadra, Z. Huang, K. Li, A. Rasmita, A. Srivastava, Z. Liu, and W.-B. Gao, Nat. Commun. **8**, 802 (2017).

[16] H. Zeng, G.-B. Liu, J. Dai, Y. Yan, B. Zhu, R. He, L. Xie, S. Xu, X. Chen, and W. Yao, Sci. Rep. **3**, 1608 (2013).

[17] G.-B. Liu, D. Xiao, Y. Yao, X. Xu, and W. Yao, Chem. Soc. Rev. **44**, 2643 (2015).

[18] T. Li and G. Galli, J. Phys. Chem. C **111**, 16192 (2007).

[19] J. He, K. Hummer, and C. Franchini, Phys. Rev. B **89**, 075409 (2014).

[20] G. Kresse and J. Furthmüller, Phys. Rev. B **54**, 11169 (1996).

[21] F. Ouyang, Z. Yang, J. Xiao, D. Wu, and H. Xu, J. Phys. Chem. C **114**, 15578 (2010).

[22] Z. Yang, J. Pan, Q. Liu, N. Wu, M. Hu, and F. Ouyang, Phys. Chem. Chem. Phys. **19**, 1303 (2017).

[23] A. Li, J. Pan, Z. Yang, L. Zhou, X. Xiong, and F. Ouyang, J. Magn. Magn. Mater. **451**, 520 (2018).

[24] P. E. Blöchl, Phys. Rev. B **50**, 17953 (1994).

[25] J. P. Perdew, K. Burke, and M. Ernzerhof, Phys. Rev. Lett. **77**, 3865 (1996).

[26] J. Neugebauer and M. Scheffler, Phys. Rev. B **46**, 16067 (1992).

[27] S. Grimme, J. Comput. Chem. **27**, 1787 (2006).

[28] G. Constantinescu, A. Kuc, and T. Heine, Phys. Rev. Lett. **111**, 036104 (2013).